Indonesian Physical Review
Volume 09 Issue 02, May 2026
P-ISSN: 2615-1278, E-ISSN: 2614-7904

Aftershock Characteristics of the 2018 Palu Earthquake: Implications for Supershear Rupture Segment

Muzli Muzli[1, 2], Karen H Lythgoe[3], Rayhan Irfan Hielmy[1], Rahmat Triyono[2], Shengji Wei[4]
[1]*State College of Meteorology, Climatology, and Geophysics (STMKG), Indonesia*
[2]*Agency for Meteorology, Climatology, and Geophysics (BMKG), Indonesia*
[3]*University of Edinburgh, United Kingdom*
[4]*Institute of Geology and Geophysics, Chinese Academy of Sciences, China*

Corresponding Author's E-mail: muzli@bmkg.go.id

Article Info

Article info:
Received: 13-02-2026
Revised: 24-05-2026
Accepted: 27-05-2026

Keywords:
Supershear rupture; Palu-Koro Fault; Aftershock pattern; Nodal array; Focal mechanism.

How To Cite:
M. Muzli, K. H. Lythgoe, R. I. Hielmy, R. Triyono, and S. Wei, "Aftershock Characteristics of the 2018 Palu Earthquake: Implications for Supershear Rupture Segment", Indonesian Physical Review, vol. 9, no. 2, p 374-385, 2026.

DOI:
https://doi.org/10.29303/ipr.v9i2.666.

Abstract

A temporary nodal array was deployed shortly after the Mw 7.5 Palu earthquake in September 2018 to record the aftershocks. Here, we present high-resolution aftershock locations and moment tensors, obtained from the temporary array combined with permanent broadband stations. The results are used to define the fault geometry and seismogenic depth. We find that there are very few aftershocks along a long, straight section of the Palu-Koro fault, which ruptured at supershear speed. Aftershocks tend to cluster north and south of this straight section. Secondary strike-slip faults to the south and east of the main fault were triggered. Additionally, we record an earthquake swarm occurring in the Adang volcanic zone, which began approximately 1 month after the mainshock. Given the smaller number and lower magnitude of aftershocks, we suggest that supershear ruptures pose a lower seismic hazard than corresponding subshear earthquakes. However, the strong shaking from a supershear rupture may pose other hazards, such as disastrous liquefaction. Lastly, we suggest that the ability to deploy short-period nodal arrays rapidly makes them a powerful tool for aftershock studies.

Copyright (c) 2026 by Author(s). This work is licensed under a Creative Commons Attribution-ShareAlike 4.0 International License.

Introduction

Supershear earthquakes, in which the rupture velocity exceeds the shear-wave velocity in the bedrock, have significant implications for seismic hazard. Models suggest that supershear rupture will influence the amount of ground shaking near the fault and affect the aftershock pattern [1], [2], [3], [4]. It has been suggested by Bouchon and Karabulut (2008) that the few supershear ruptures observed in nature exhibit a characteristic aftershock pattern, with aftershocks clustering on secondary faults away from the main fault, a phenomenon also observed in laboratory settings, where fault roughness controls aftershock productivity [5].

However, the aftershocks analyzed by [6] were from a global earthquake catalog, which has considerable location uncertainty and excludes small-magnitude events.

The Mw7.5 Palu 2018 earthquake in Sulawesi was a supershear earthquake [7], [8]. The earthquake ruptured part of the Palu-Koro fault - a left-lateral strike-slip fault running from the subduction trench in the Celebes Sea to terminate onshore in Sulawesi. The Mw 7.5 earthquake triggered deadly cascading hazards, including a tsunami [9], submarine landslides [10], and large-scale liquefaction [11], severely impacting Palu's urban infrastructure [12], [13]. Advanced 3D acoustic-elastic coupled simulations have further highlighted the complex dynamics between the fault rupture and the resulting tsunami generation[14]. Geodetic data from GNSS stations confirmed extreme divergent left-lateral movement during the co-seismic phase [15].

Being long and straight with a high slip rate, the fault was previously recognized as being a candidate for supershear rupture [16]. Teleseismic back-projection analysis indicates that at least part of the rupture was supershear [7]. Nevertheless, it remains uncertain whether this supershear rupture speed manifested across the whole length of the fault immediately upon the earthquake's initiation, or if it developed subsequently along a localized fault segment [8]. Joint analyses of InSAR and broadband seismograms further corroborate this supershear mechanism and provide detailed constraints on the multi-segment source characteristics of the rupture [17], [18].

A network of short-period seismic nodes was rapidly deployed in the aftermath of the M7.5 Palu event to capture the ensuing aftershock sequence. The logistical efficiency of these instruments makes such temporary arrays perfectly suited for investigating fault ruptures in territories with limited seismic monitoring infrastructure [19]. Furthermore, highly dense nodal arrays have proven effective for detecting microseismicity even in noisy urban environments [20] and analyzing detailed spatial correlations of ground motion [21]. The locations of the nodes were designed to complement existing permanent broadband stations. Here, we report high-resolution aftershock locations and moment tensors for the Palu-Koro fault and its surroundings. We define the fault geometry and seismogenic depth and show the aftershock distributions along a long, straight segment of the fault. We investigate the segment that ruptured with supershear speed.

Data and Methods

Seismic Array

Twenty short-period nodes were deployed within nine days following the mainshock. The locations were designed to fill in gaps in the existing permanent network of broadband seismic stations operated by the Agency for Meteorology, Climatology, and Geophysics of Indonesia (BMKG) and Helmholtz-Zentrum für Geoforschung (GFZ-Potsdam). In total, 61 seismic stations were used in the analysis, with an average spacing of approximately 40 km. Most of the stations are located on the Celebes Islands. The stations are well distributed so as to provide coverage of the identified faults in the region. The permanent seismic stations owned by BMKG have a relatively better quality compared to the short-period temporary seismic stations in terms of the location. Figure 1 shows the locations of all stations used in

this analysis. The nodes recorded for 35 days (Figure 2) which is the extent of their battery life.

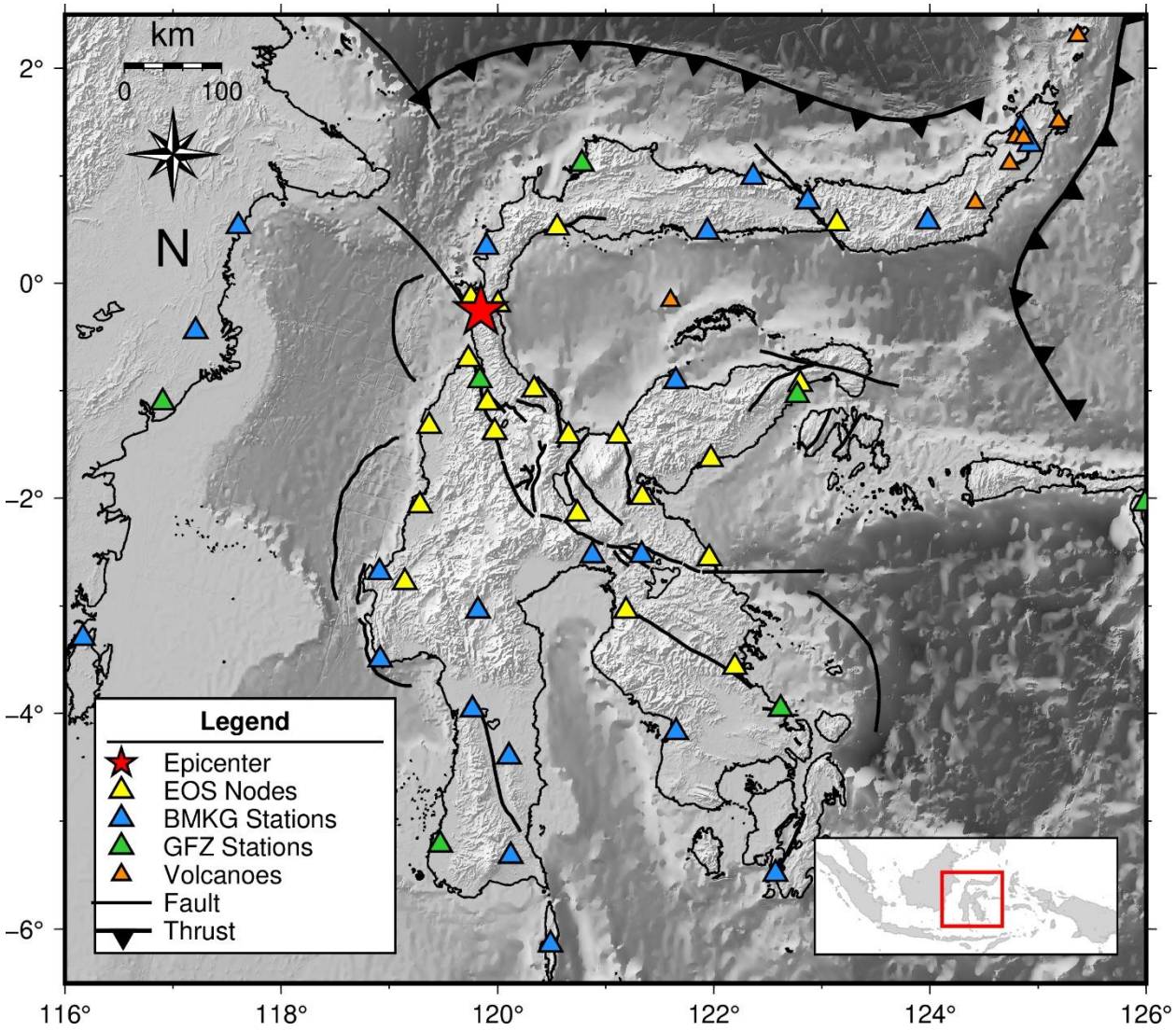

Figure 1. Map of Sulawesi, the seismic stations used in the aftershock analysis. The seismic array is composed of twenty temporary short-period nodes deployed by the Earth Observatory of Singapore (EOS) and the Agency for Meteorology, Climatology, and Geophysics (BMKG) (EOS Nodes, yellow triangles), permanent broadband seismic stations of BMKG (blue triangles), and permanent broadband stations of GFZ-Potsdam (green triangles). The red star marks the hypocenter of the mainshock. Black lines indicate quaternary faults mapped by Watkinson & Hall (2017). Orange triangles are Holocene volcanoes.

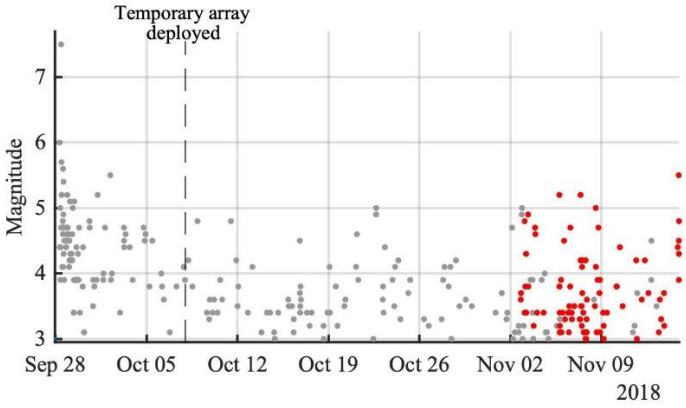

Figure 2. Timeline of aftershocks from the Mw7.5 main event. Red circles are earthquakes from the swarm to the south-west of the Palu-Koro fault.

Aftershock relocation

We begin with initial event locations from the catalog of the Agency for Meteorology, Climatology, and Geophysics of Indonesia (BMKG), followed by manual searches for events in continuously recorded waveforms from the temporary networks. We re-locate the events using a double difference relative relocation method [22]. To ensure a high-quality travel-time database, we handpick and quality-control the P-wave arrival times at all stations that were active at the time of the event. This study prioritized meticulous detection via relative relocation to ensure high-resolution data. We then relocate all events together. Before the temporary nodal array was active, we had arrivals only from the permanent stations; the relative relocation method ensures that these events are accurately located with respect to events recorded by the nodal array. We use a 1D velocity model extracted from the model of [23] and assume a Vp/Vs ratio of 1.73. The relative event relocation reduces dependence on the velocity model; we also investigate velocity-model uncertainties in a later section. Other approaches to map the Palu-Koro seismicity include non-linear hypocenter localization [24] and fractal analysis for hypocenter dimensions [25]. Interestingly, we observed that the aftershock seismicity pattern followed the rupture's directivity. The cross-section reveals a distinct seismicity alignment dipping towards the south, consistent with the rupture directivity shown in Figure 3.

Focal Mechanism

We derive focal mechanisms of aftershocks by waveform modeling using the cut-and-paste method [26]. The cut-and-paste method separates the wavefield into Pnl and surface-wave segments, which are inverted independently, thereby reducing sensitivity to the 1D velocity model. The earthquake is treated as a point source, a reasonable assumption given the magnitudes of the aftershocks. Before waveform inversion, it is critical to remove the instrument response. Removing the instrument response for node instruments allows much longer recovery periods, and we can confidently recover a signal with a period as low as 20 seconds.

We also incorporate records from the broadband permanent seismic network into the focal mechanism inversion. To combine the broadband and short-period nodes, we apply station-dependent waveform filtering. For example [27], typical waveform bandpass filtering ranges

for Pnl waves are 0.05-0.16 Hz for nodes and 0.01-0.06 Hz for broadband stations; and for surface waves, 0.05 – 0.12 Hz for nodes and 0.01 – 0.035 Hz for broadband stations.

Figure 4 shows an example of waveform fitting using the short-period nodes and broadband permanent stations for an aftershock on the main Palu-Koro fault. The use of short-period nodes limits the lowest frequency available for these stations, making the waveforms more sensitive to the velocity model. Fortunately, by incorporating broadband permanent stations, we obtain robust focal mechanisms for the aftershocks, as indicated by the quality of waveform fits between observed and synthetic data (Figure 4). We use residual values from waveform fitting between the observed and synthetic data to evaluate the quality of the focal mechanism inversion.

Result and Discussion

Aftershock locations

Figure 3 shows the relocated aftershocks. Compared to standard catalogs, such as the catalog we begin with, the aftershocks are more spatially consistent. The depth of the mainshock is relocated from 25 km to 14 km, and the majority of aftershocks occur at depths less than 14 km, indicating the seismogenic depth in the region. This is broadly consistent with a fault locking depth estimated by geodetic methods to be approximately 12 km [28], [29], [30].

There is a distinct gap in seismicity within Palu Bay and the Palu Valley (Figure 3), where the geometry of the main Palu-Koro fault is straight [31]. Despite this aftershock gap, recent SAR interferometry studies indicate that the offshore section in Palu Bay actively participated in the multi-segment rupture process [32]. Such straight sections on strike-slip faults are thought to host supershear rupture [33].This location coincides with where high-frequency point source back projections indicate earthquake rupture exceeded shear wave speed [7]. Thus, we conclude that relatively few aftershocks occurred along the section of the Palu-Koro fault that ruptured with supershear speed. Most aftershocks cluster north and south of this section.

The relocations show that several secondary faults were triggered (Figure 3). The triggering of secondary faults may be due to high stresses transferred from the sonic boom during supershear rupture [6], consistent with Coulomb stress modeling, which shows increased stress lobes in these areas [34]. Events to the east of the Palu-Koro fault occur within the Sapu valley fault system. The Sapu valley fault system is a sequence of NW-SE-trending faults, and its activity level was previously unknown [16]. The moment tensor indicates a steeply dipping strike-slip fault.

Events to the south-east of the Palu-Koro fault show that the Matano fault was also triggered. Additionally, a Mw 6.8 event occurred on the Matano fault, approximately 300 km to the southeast of the Palu main earthquake on 4th December 2019, 2 months after the main Palu earthquake. The Matano fault may be connected to the southern termination of the Palu-Koro fault, as suggested by rigid block models [28]. Similar complex rupture interactions and doublet events were recently observed in the 2023 Kahramanmaraş sequence [35], suggesting a global characteristic of supershear fault systems.

A cluster of earthquakes to the south-west began over one month after the main shock (red events in Figure 2; location shown in Figure 3). The close spatial clustering of events and their

migration, along with the absence of a main event, are indicative of an earthquake swarm. Such non-volcanic swarms are often driven by fluid diffusion or aseismic slip transients [36]. Although such swarms are often associated with fluid movement in the crust at volcanoes, there is no active volcanism in this area (Figure 1). The swarm is located in the Adang Cenozoic volcanic zone – extrusive rocks of unknown age which formed during a period of rifting [37] – and the swarm is located at the northern terminus of the Walanae strike-slip fault (Figure 3). Focal mechanisms show strike-slip and normal faulting. Although this area is prone to frequent seismicity, it is poorly studied and will be the focus of future work.

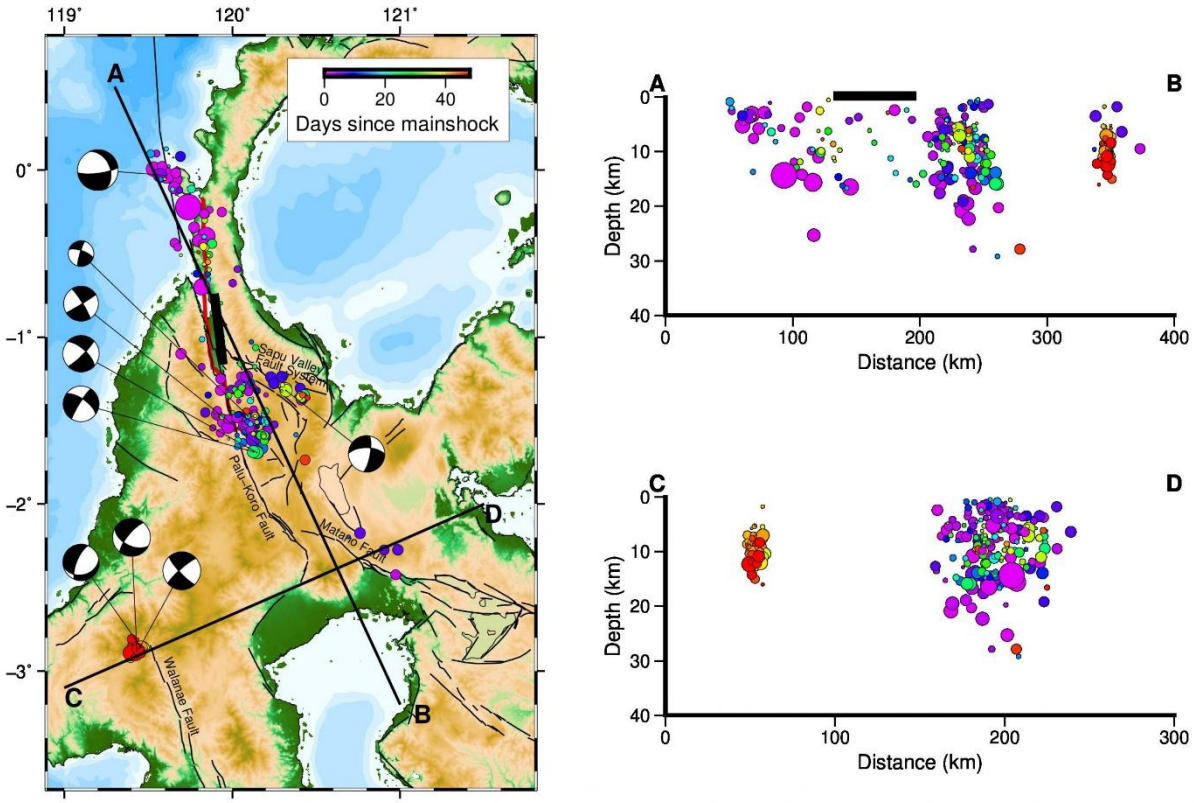

Figure 3. Earthquake relocations and moment tensors obtained by waveform inversion. The thick black line indicates the inferred supershear rupture segment.

Aftershock location uncertainty

Earthquake location uncertainty is due to several factors, including station coverage, event distribution, and the velocity model (Figure 5). To estimate location uncertainty due to station and event distribution, we employ bootstrap resampling. For stations, this means removing one station at a time and relocating the events. For events, this means removing a random 5% of events and repeating the relocation. This iterative resampling procedure continues until every individual station or event has been excluded from at least one recalculated dataset. Location uncertainty is subsequently defined as the maximum spatial deviation between the hypocenter derived from the complete dataset and the scattered distribution of the resampled

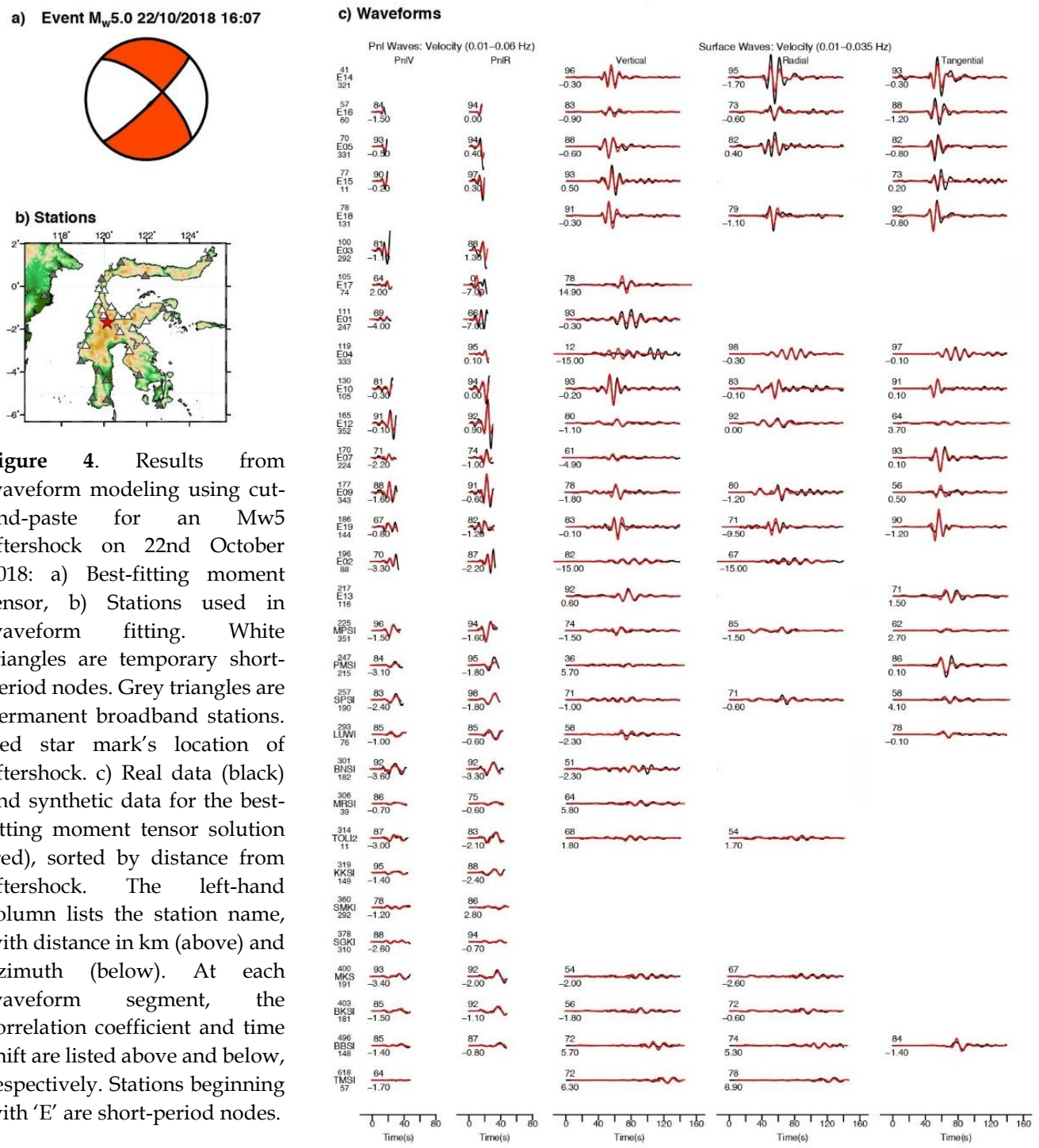

Figure 4. Results from waveform modeling using cut-and-paste for an Mw5 aftershock on 22nd October 2018: a) Best-fitting moment tensor, b) Stations used in waveform fitting. White triangles are temporary short-period nodes. Grey triangles are permanent broadband stations. Red star mark's location of aftershock. c) Real data (black) and synthetic data for the best-fitting moment tensor solution (red), sorted by distance from aftershock. The left-hand column lists the station name, with distance in km (above) and azimuth (below). At each waveform segment, the correlation coefficient and time shift are listed above and below, respectively. Stations beginning with 'E' are short-period nodes.

points. We also investigate uncertainty arising from the velocity model by performing relocation using several reference 1D velocity models (PREM [38] and IASPI91 [39]). The uncertainty range for each event is estimated as the maximum distance between the relocations obtained from the different velocity models.

Aftershock magnitudes

Despite the large magnitude of the main shock, the aftershocks are relatively small. The largest magnitude aftershock was Mw 5.6 (Figure 2), which is lower than expected for a main shock of this size [40] . Additionally, very few aftershocks were recorded along the supershear rupture segment in the 1.5 months following the main shock (Figure 3). Low-magnitude aftershocks may be a key feature of all supershear ruptures, since most of the energy is released during the main shock. Bouchon & Karabulut (2008) Show that, following the supershear rupture of the Mw 7.9 Kunlunshan, Tibet earthquake, the largest aftershock magnitude was Mw 5.6. They also show a similarly low number and magnitude of aftershocks following the supershear ruptures of Mw7.4, 1999 Izmit earthquake; the 1999, Mw 7.2 Duezce earthquake; and the 2002, Mw7.9 Denali earthquake.

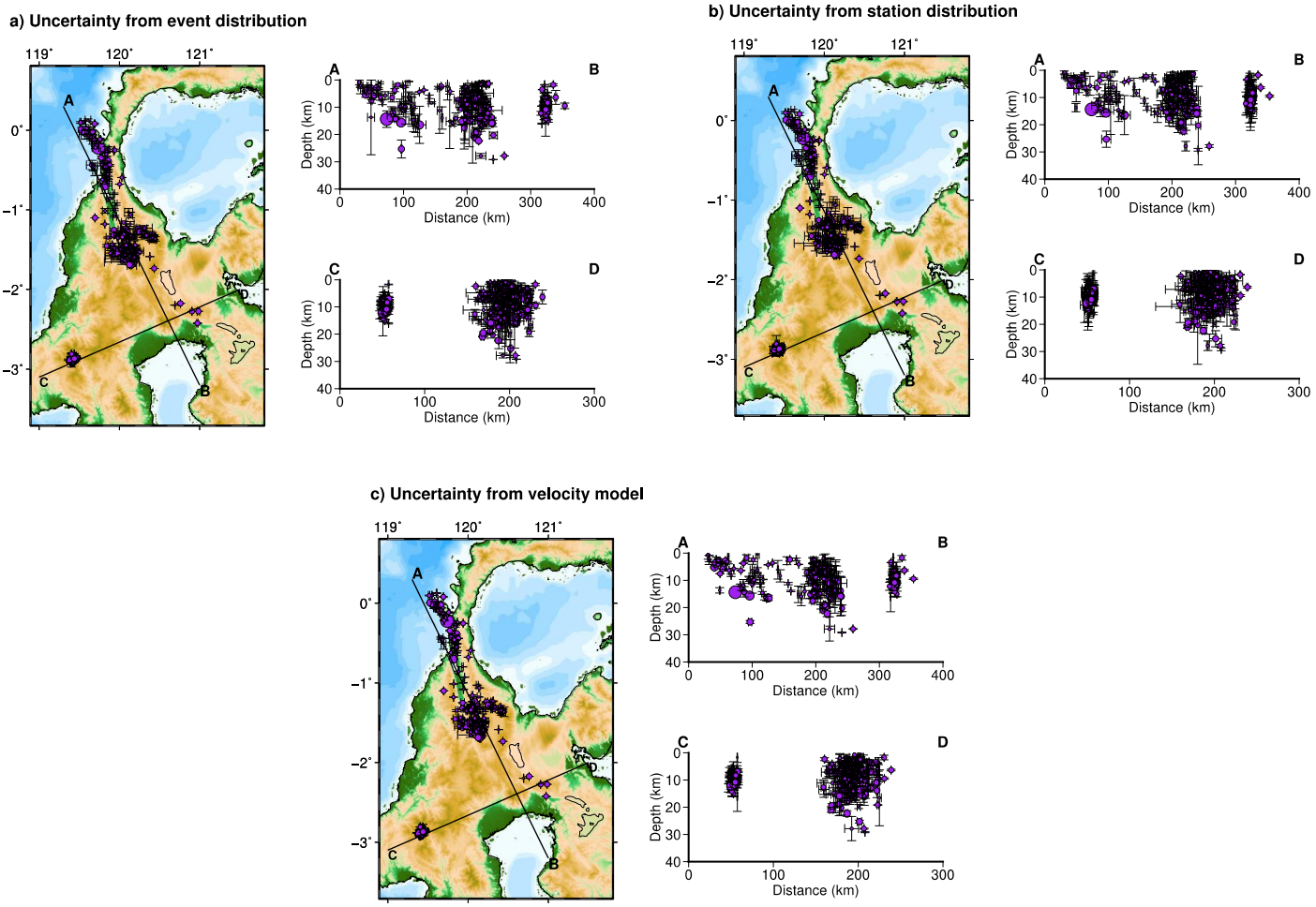

Figure 5. Event location uncertainty resulting from a) event distribution, b) station distribution, and c) velocity model.

Conclusion

By deploying a temporary array to record the aftershock pattern, we can obtain high-resolution aftershock locations that delineate the rupture trace and define the fault geometry and seismogenic depth. We find that there are relatively few aftershocks along a long, straight section of the Palu-Koro fault, suggesting that this segment ruptured at supershear speed. Aftershocks tend to cluster north and south of this straight section. We suggest that supershear ruptures may, in fact, be safer than corresponding subshear earthquakes in terms of aftershocks, due to their fewer and lower magnitude aftershocks, although the strong shaking of supershear ruptures may produce other hazards, such as liquefaction. Secondary faults were triggered, possibly due to high stress transfer during the sonic boom of a supershear rupture. Lastly, the short-period nodes used in the temporary array could be deployed easily and rapidly; we suggest that nodal arrays will play a powerful role in future earthquake aftershock studies. This study demonstrates that rapid deployment of short-period nodal arrays is a cost-effective and powerful strategy for capturing detailed aftershock patterns in complex fault zones like Sulawesi, highlighting the critical role of rapid response networks in modern seismology [41].

Acknowledgements

We thank Wardah Fadil, Qibin Shi, Weiwen Chen, and Phyo Maung Maung for assistance with arrival-time picking, and BMKG, EOS, and GFZ for providing seismic data. Dr. Ian Watkinson provided fault traces. Maps were made using GMT [42].

References

[1] K. Chen, G. Wei, C. Milliner, C. Liang, J. Avouac, and L. D. Zilio, "Super-shear ruptures steered by pre-stress heterogeneities during the 2023 Kahramanmara ş earthquake doublet," *Nat. Commun.*, vol. 15, pp. 1–11, 2024.

[2] Z. Zhang, J. Xu, H. Huang, and X. Chen, "Seismic characteristics of supershear and sub-Rayleigh earthquakes : Implication from simple cases," *Geophys. Res. Lett.*, vol. 44, pp. 6712–6717, 2017.

[3] P. Bernard and D. Baumont, "Shear Mach wave characterization for kinematic fault rupture models with constant supershear rupture velocity," *Geophys. J. Int.*, vol. 162, pp. 431–447, 2005.

[4] E. M. Dunham and R. J. Archuleta, "Near-Source Ground Motion from Steady State Dynamic Rupture Pulses," *Geophys. Res. Lett.*, vol. 32, no. 3, 2004.

[5] T. H. W. Goebel, E. E. Brodsky, and G. Dresen, "Fault Roughness Promotes Earthquake-Like Aftershock Clustering in the Lab Geophysical Research Letters," *Geophys. Res. Lett.*, vol. 50, no. 8, pp. 1–11, 2023.

[6] M. Bouchon and H. Karabulut, "The Aftershock Signature of Supershear Earthquakes," *Science (80-.).*, vol. 320, no. 5881, pp. 1323-1325, 2008.

[7] H. Bao *et al.*, "Early and persistent supershear rupture of the 2018 magnitude 7 . 5 Palu earthquake," *Nat. Geosci.*, vol. 12, no. 3, pp. 200–205, 2025.

[8] A. Socquet *et al.*, "Evidence of supershear during the 2018 magnitude 7.5 Palu earthquake

from space geodesy," *Nat. Geosci.*, vol. 12, no. 3, pp. 192–199, 2019.

[9] W. Simons *et al.*, "A Tsunami Generated by a Strike-Slip Event : Constraints From GPS and SAR Data on the 2018 Palu Earthquake," *J. Geophys. Res. Solid Earth*, vol. 127, no. 12, 2022.

[10] M. G. Cilia, W. D. Mooney, and C. Nugroho. "Field Insights and Analysis of the 2018 Mw 7 . 5 Palu, Indonesia Earthquake, Tsunami and Landslides," *Pure Appl. Geophys.*, vol. 178, no. 12, pp. 4891–4920, 2021.

[11] T. Kiyota, H. Furuichi, R. Faris, N. Tada, and H. Nawir, "Overview of long-distance flow-slide caused by the 2018 Sulawesi earthquake, Indonesia," *Soils Found.*, vol. 60, no. 3, pp. 722–735, 2020.

[12] A. Triyanti *et al.*, "Governing systemic and cascading disaster risk in Indonesia: where do we stand and future outlook Annisa," *Disaster Prev. Manag. An Int. J.*, vol. 32, no. 1, pp. 27–48, 2026.

[13] S. Al Idrus, "Political Change and Urban Growth in a Medium-sized Outer Island Capital in Indonesia : The Case of Palu, Central Sulawesi Dissertation for the award of the degree " Doctor rerum naturalium " of the Georg-August-Universität Göttingen within the doctoral," Georg-August-Universität Göttingen, 2022.

[14] L. Krenz *et al.*, "3D Acoustic-Elastic Coupling with Gravity : The Dynamics of the 2018 Palu, Sulawesi Earthquake and Tsunami," in *Proceedings of the International Conference for High Performance Computing, Networking, Storage and Analysis*, 2021, pp. 1–14.

[15] Nurdin, Marzuki, D. Arisa, and V. Friska, "Seismic Deformation Analysis of the 28th September 2018 Palu Earthquake (7 . 5 Mw) Using InaCORS Station Data and Okada Model," *J. Penelit. Pendidik. IPA*, vol. 10, no. 4, pp. 2154–2161, 2024.

[16] I. M. Watkinson and R. Hall, "Fault systems of the eastern Indonesian triple junction: Evaluation of Quaternary activity and implications for seismic hazards," *Geol. Soc. Spec. Publ.*, vol. 441, no. 1, pp. 71–120, 2017.

[17] J. Fang, C. Xu, Y. Wen, S. Wang, G. Xu, and Y. Zhao, "The 2018 Mw 7 . 5 Palu Earthquake : A Supershear Rupture Event Constrained by InSAR and Broadband Regional Seismograms," *Remote Sens.*, vol. 11, no. 11, pp. 1–15, 2018.

[18] Y. Wang, W. Feng, K. Chen, and S. Samsonov, "Source Characteristics of the 28 September 2018 Mw 7 . 4 Palu, Indonesia, Earthquake Derived from the Advanced Land Observation Satellite 2 Data," *Remote Sens.*, vol. 11, no. 11, pp. 1–16, 2019.

[19] J. Yao, D. Yao, F. Chen, M. Zhi, L. Sun, and D. Wang, "Editorial A Preliminary Catalog of Early Aftershocks Following the 7 January 2025 M S 6 . 8 Dingri, Xizang Earthquake," *J. Earth Sci.*, vol. 36, no. 2, pp. 856–860, 2025.

[20] J. Omojola and P. Persaud, "Detecting Urban Earthquakes with the San Fernando Valley Nodal Array and Machine Learning," *Seismol. Res. Lett.*, vol. 97, no. 1, pp. 111–125, 2026.

[21] Y. Sheng, Q. Kong, and G. C. Beroza, "Network analysis of earthquake ground motion spatial correlation : a case study with the San Jacinto seismic nodal array," *Geophys. J. Int.*, vol. 225, pp. 1704–1713, 2021.

[22] F. Waldhauser and W. L. Ellsworth, "A Double-difference Earthquake location algorithm:

Method and application to the Northern Hayward Fault, California," *Bull. Seismol. Soc. Am.*, vol. 90, no. 6, pp. 1353–1368, 2000.

[23] N. A. Simmons, S. C. Myers, and G. Johannesson, "LLNL-G3Dv3 : global P-wave tomography model for improved regional and teleseismic travel time prediction," *J. Geophys. Res.*, vol. 117, no. B10, 2012.

[24] H. Jayadi, G. Rachman, I. U. Meidji, M. Fawzy, I. Massinai, and D. D. Warnana, "A Non-Linear Hypocenter Localization along the Active Palu- Koro Fault: A Case Study, Central Sulawesi," *Indonesian Physical Review, vol.* 08, no. 02, pp. 400–416, 2025.

[25] S. Rasimeng *et al.*, "Hypocenter dimension of 7 . 5 mw Palu earthquake using fractal approach Hypocenter dimension of 7 . 5 mw Palu earthquake using fractal approach," in *IOP Conference Series: Earth and Environmental Science*, 2020, pp. 1–10.

[26] L. Zhu and D. V Helmberger, "Advancement in Source Estimation Techniques Using Broadband Regional Seismograms," *Bull. Seismol. Soc. Am.*, vol. 86, no. 5, pp. 1634–1641, 1996.

[27] Li, Xiaobin, Mingpei Jin, Ya Huang, Wenjian Cha, Jun Wang, and Sihai Li. "Temporal evolution of the focal mechanism consistency of the 2021 Yangbi MS 6.4 earthquake sequence in Yunnan." Earthquake Research Advances 2, no. 2, 2022.

[28] A. Socquet *et al.*, "Microblock rotations and fault coupling in SE Asia triple junction (Sulawesi, Indonesia) from GPS and earthquake slip vector data," *J. Geophys. Res.*, vol. 111, pp. 1–15, 2006.

[29] C. Stevens, R. McCaffrey, C. Subarya, and C. Vigny, "Rapid rotations about a vertical axis in a collisional setting revealed by the Palu fault, Sulawesi, Indonesia," *Geophys. Res. Lett.*, vol. 26, no. 17, pp. 2677–2680, 1999.

[30] A. Walpersdorf and P. Manurung, "Monitoring of the Palu-Koro Fault (Sulawesi) by GPS," *Geophys. Res. Lett.*, vol. 25, no. 13, pp. 2313–2316, 1998.

[31] D. H. Natawidjaja *et al.*, "The 2018 Mw7.5 Palu 'supershear' earthquake ruptures geological fault's multisegment separated by large bends: Results from integrating field measurements, LiDAR, swath bathymetry and seismic-reflection data," *Geophys. J. Int.*, vol. 224, no. 2, pp. 985–1002, 2021.

[32] G. Bacques, M. De Michele, M. Foumelis, D. Raucoules, A. Lemoine, and P. Briole, "Sentinel optical and SAR data highlights multi-segment faulting during the 2018 Palu-Sulawesi earthquake (M w 7 . 5)," *Sci. Rep.*, pp. 1–11, 2020.

[33] A. Ansal, *Perspectives on European Earthquake Engineering and Seismology*, vol. 2. Springer Nature, 2015.

[34] B. Ahadov and J. Sh, "The Impact of Coulomb Stress Changes of the 2018 Mw 7.5 Palu Earthquake, Indonesia," *Earth Sci.*, vol. 2, pp. 14–25, 2023.

[35] L. D. Zilio and J. Ampuero, "Earthquake doublet in Turkey and Syria," *Commun. Earth Environ.*, vol. 4, no. 1, pp. 2–5, 2023.

[36] Y. Yukutake, K. Yoshida, and R. Honda, "Interaction Between Aseismic Slip and Fluid Invasion in Earthquake Swarms Revealed by Dense Geodetic and Seismic Observations," *J. Geophys. Res. Solid Earth*, vol. 127, no. 4, pp. 1–18, 2022.

[37] G. Shaban and B. Priadi, "Geochemical Signatures of Potassic to Sodic Adang Volcanics, Western Sulawesi : Implications for Their Tectonic Setting and Origin. Large parts of the Western Sulawesi Province are covered by thick (up to 5000 m) piles of Upper Cenozoic shoshonitic to." *Indones. J. Geosci.*, vol. 3, no. 3, pp. 197–216, 2021.

[38] A. M. Dziewonski and D. L. Anderson, "Preliminary reference Earth model," *Phys. of the Earth and Planetary Inter.*, vol. 25, pp. 297–356, 1981.

[39] B. L. N. Kennett and E. R. Engdah, "Traveltimes for global earthquake location and phase identification," *Geophys. J. Int.*, vol. 105, pp. 429–465, 1991.

[40] P. A. Reasenberg and L. M. Jones, "Earthquake aftershocks: update." *Science (80-), vol.* 265, no. 5176, pp. 1251–1253, 1994.

[41] R. Fonzetti, A. Govoni, P. De Gori, and C. Chiarabba, "earthquake with ML methods," *Geophys. J. Int.*, vol. 239, pp. 99–111, 2024.

[42] P. Wessel *et al.*, "The Generic Mapping Tools Version 6," *Geochemistry, Geophys. Geosystems*, vol. 20, no. 11, pp. 5556–5564, 2019.